ARCHIVIO ISTITUZIONALE DELLA RICERCA

Alma Mater Studiorum Università di Bologna
Archivio istituzionale della ricerca

Liquid mixing time and gas distribution in aerated multiple-impeller stirred tanks

This is the final peer-reviewed author's accepted manuscript (postprint) of the following publication:

*Published Version:*
Liquid mixing time and gas distribution in aerated multiple-impeller stirred tanks / Zak A.; Alberini F.; Maluta F.; Moucha T.; Montante G.; Paglianti A.. - In: CHEMICAL ENGINEERING RESEARCH & DESIGN. - ISSN 0263-8762. - STAMPA. - 184:(2022), pp. 501-512. [10.1016/j.cherd.2022.06.021]

*Availability:*
This version is available at: https://hdl.handle.net/11585/889944 since: 2022-09-01

*Published:*

DOI: http://doi.org/10.1016/j.cherd.2022.06.021

*Terms of use:*

Some rights reserved. The terms and conditions for the reuse of this version of the manuscript are specified in the publishing policy. For all terms of use and more information see the publisher's website.

This item was downloaded from IRIS Università di Bologna (https://cris.unibo.it/).
When citing, please refer to the published version.

(Article begins on next page)

27 April 2024

This is the final peer-reviewed accepted manuscript of:

Liquid mixing time and gas distribution in aerated multiple-impeller stirred tanks | Elsevier Enhanced Reader [WWW Document], n.d.

The final published version is available online at: https://doi.org/10.1016/j.cherd.2022.06.021

Rights / License:

The terms and conditions for the reuse of this version of the manuscript are specified in the publishing policy. For all terms of use and more information see the publisher's website.

*This item was downloaded from IRIS Università di Bologna (https://cris.unibo.it/)*

***When citing, please refer to the published version.***

# Liquid mixing time and gas distribution in aerated multiple-impeller stirred tanks

A. Zak[1], F. Alberini[2], F. Maluta[2], T. Moucha[1], G. Montante[2], A. Paglianti[2*]

[1]University of Chemistry and Technology Prague, Department of Chemical Engineering, Technicka 5., 16628 Prague, Czech Republic

[2]Department of Industrial Chemistry 'Toso Montanari', University of Bologna, via Terracini 34, 40131, Bologna, Italy

**Abstract**

Gas-liquid fluid dynamics and mass transfer are crucial aspects of aerobic fermentation and robust methodologies for their determination in industrial bioreactors are expected to provide significant improvements in many production processes. In this work, a gas-liquid stirred tank of high aspect ratio, that replicates the geometry of typical industrial aerated fermenters, is investigated. In particular, the liquid phase homogenization dynamics and the gas phase spatial distribution are determined. The selected methodology is based on the analysis of the conductivity measurements obtained by Electrical Resistance Tomography. The gas-liquid flow regimes and the mixing time are identified at various gas flow rates and impeller speeds, thus covering different gas-liquid regimes. Data collected with vertical and horizontal arrangements of the electrodes allow to obtain a detailed picture of the equipment working mode and to gain insight into the gas-liquid flow dynamics under optically inaccessible conditions. Quantitative evaluation of the reliability of the collected data is attempted by comparing the results obtained with the vertical and horizontal arrangements in the same locations.

Keywords: Stirred tank, Flow regimes, Gas-liquid, ERT, Mixing time, Multiple-impeller

* Corresponding Author Prof. A. Paglianti, e-mail: alessandro.paglianti@unibo.it

## 1. Introduction

Mass transfer issues related to the non-ideal fluid dynamics are common in industrial gas-liquid operations. For instance, deviations from completely dispersed gas conditions often occur when the gas flow rate is increased to increase the mass transfer rate. If the flow regime moves from completely dispersed or loading to flooding conditions, the increment of the gas flow rate results in a decrement of the mass transfer rate and longer mixing times. The capability to account for the interplay among hydrodynamics, mixing and mass transfer variables are industrially relevant for translating results from lab to pilot and commercial scales (Abdullah and Adesina, 2017) in several applications. It is the case for instance of aerobic fermentations, especially when high oxygen uptake rates are required and the production rate is limited by oxygen supply or liquid mixing (Noorman et al., 2018). Current knowledge on gas-liquid stirred tanks is deeper in the case of dilute systems since most experimental methods are limited to transparent media. At high gas hold-up and under turbulent conditions experimental data useful for computational model validation are difficult to obtain (Cappello et al., 2021). Therefore, correlations among global parameters are mainly adopted for the design and scale-up of the stirred chemical and biochemical reactors. Many uncertainties still affect the prediction of key variables, such as liquid mixing time in gassed stirred tanks. Depending on the relative importance of the energy transfer from the bubbles to the liquid and the impeller power consumption, either an increase or a decrease in the mixing time due to aeration can be obtained (Zhao et al., 2001). Generally, uncertainties on scale-up of gas-liquid fermenters have reduced the application of biological productions in the case of high value compounds like pharmaceutical or speciality chemicals (Humbird et al., 2017). In this context, reliable predictive methods can reduce the current uncertainties affecting the scale-up of industrial reactors, but robust validation with experimental data is still required for their comprehensive application. Besides techniques requiring high energy radiation, such as X-ray (Ford et al., 2008) and γ-ray Tomography (Veera et al., 2001), which have proved very effective in gas-liquid mixing investigations, Electrical Resistance Tomography (ERT) was identified as a viable technique for providing a fair representation of aerated stirred tanks with relatively simple and cheap instrumentation. Applications of ERT for the characterization of gas-liquid mixing concerns for instance pilot reactors (Wang et al., 2000) and tanks stirred with coaxial impellers (Jamshidzadeh et al., 2021). In addition, ERT has been recently adopted in combination with other measurement methods (Forte et al., 2021). The applicability of ERT has been also estimated in different gas-liquid systems, such as air-water flows in vertical pipes

(Olerni et al., 2013), bubbly gas-liquid horizontal channels (Deng et al., 2001), bubble columns (Babaei et al., 2015). Recently, Forte et al. (2019) have applied ERT to the determination of gas hold-up distribution in a laboratory stirred tank, finding a lower accuracy of the results collected with a linear probe with respect to X-ray computed tomography. In this work, ERT is applied to the investigation of a pilot gas-liquid stirred tank adopting different configurations of the electrodes to investigate the capability of the technique in providing not only a qualitative picture but also quantitative results on crucial variables for the understanding and the optimization of gas-liquid operations.

## 2. Experimental

The investigated pilot-scale baffled stirred tank, schematically shown in Figure 1, consisted of a cylindrical, flat bottomed vessel of diameter, T, equal to 0.48 m and height, H, equal to 1.6 m, equipped with four equally spaced baffles of width, W, equal to T/10. To evaluate the gas dispersion features, a standard configuration, which is often adopted for industrial aerobic fermentations, has been considered. Agitation was provided with three identical Rushton turbines with diameter, D, equal to 0.19 m (D=0.40T), the lower one was set at an off-bottom clearance, C, of T/2 and the distance between two consecutive impellers was equal to T. The impeller speed, N, and the gas flow rate, $Q_G$, were changed in the range of 50-500 rpm and 0-200 L $min^{-1}$, respectively. The gas flow rate covers a range of superficial gas velocities of 0-0.018 m/s, corresponding to 0-0.7 vvm. In all the experiments, the tank was filled with a dilute solution of sodium chloride in demineralised water up to a height, $H_L$, equal to 1.39 m. Afterwards, air was sparged in water through a ring sparger of diameter, $D_s$, equal to 0.09 m ($D_s$=0.47D) provided with 36 equally spaced holes of 2 mm in diameter and located at clearance with respect to the vessel bottom, $C_s$, equal to 85 mm ($C_s$ =0.18T).

The mixing time and the gas hold-up distribution were determined on three horizontal planes and one vertical plane by using an ITS P2000 ERT instrumentation by Industrial Tomography Systems Ltd. Both in the vertical and the horizontal arrangement, 16 equally spaced electrodes were adopted, as schematized in Figure 1. The electrodes were squared stainless steel plates of 30 mm side and 1 mm thickness, fixed to the vessel wall. The distance between two consecutive electrodes in the vertical arrangement was equal to 60 mm, with the bottom electrode placed at $z_B$=180 mm and the top one at $z_T$=1080 mm from the vessel bottom. In the horizontal arrangement 16 electrodes per plane were equally spaced along the vessel periphery at the axial elevations, $z_1$, $z_2$, and $z_3$ of 420 mm ($z_1$=0.875T), 900 mm ($z_2$=1.875T) and 1260 mm

($z_3$=2.625T) from the vessel bottom. The electrodes were connected to the data acquisition system (DAS) by coaxial cables.

The measurements were based on the adjacent strategy, in which electric current is injected from adjacent electrodes pair at a time and the voltage difference is measured from the remaining pairs of electrodes. The procedure is repeated for all the independent pairs of electrodes. The injected current was always of 15 mA and the frequency was fixed at 9600 Hz. The conductivity maps were reconstructed from the electric potential measurements by the linearized (non-iterative) modified sensitivity back projection (MSBP) algorithm, as implemented in the ITS System p2+ V8 software.

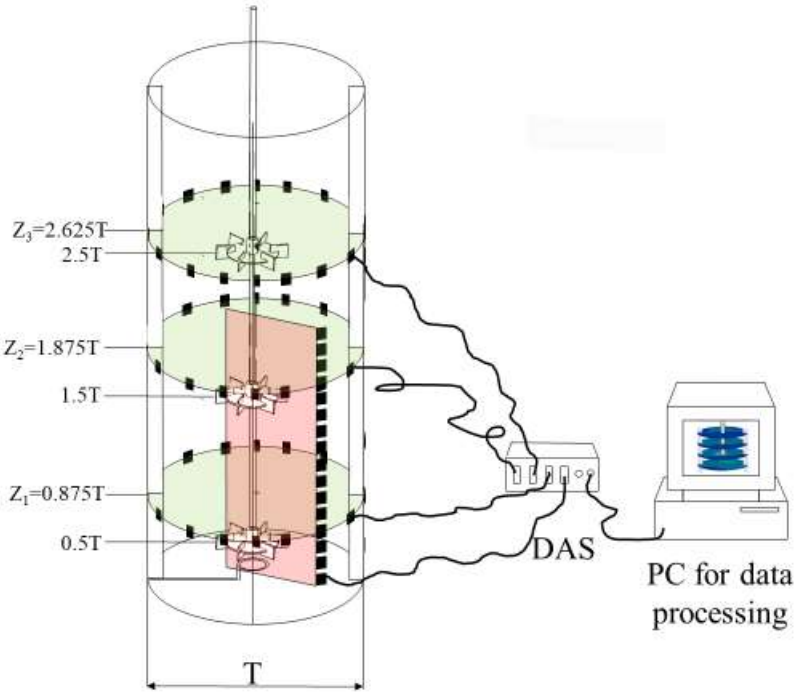


Figure 1 Schematic characteristics of the experimental system. Highlighted the horizontal measurement sections (green) and the vertical measurement section (red)

The raw ERT data consisted of either circular or rectangular conductivity maps, depending on electrode arrangement. In the case of horizontal measurements, the spatial resolution on each plane can be simply identified, since the 316 conductivity values are located in a circle of diameter equal to 480 mm, therefore the local conductivity on each plane was obtained on a mesh with cells of 20 mm x 20 mm. For the vertical arrangement, 160 conductivity values were used, they are located in front of the 16 electrodes on horizontal lines each with 10 cells in the radial direction. The vertical resolution can be identified from the distance of two consecutive

electrodes, which is 60 mm, the horizontal resolution was estimated equal to 36 mm, by using a phantom consisting of a non-conductive rod of 30 mm in diameter. The rod was placed at four different radial positions and maintained always parallel to the vessel axis. For avoiding electrical disturbances, the shaft and the impellers were preliminarily removed. In this way, the final dimensions of the vertical tomogram were determined. The vertical plane covers an area of an approximate dimension of 360 mm in the radial direction by 900 mm in the axial direction. For each combination of impeller speed and gas flowrate, the experiments with the gas-liquid mixtures have been repeated adopting the vertical arrangement first and the horizontal one subsequently.

## 2.1 Mixing time and gas hold-up measurement strategies

In the following, the methodologies to obtain the dimensionless local conductivity, which is computed as the ratio between the local conductivity and a reference conductivity, are described. Depending on the measurement target, namely the mixing time or the gas hold-up, different acquisition procedures for the local and the reference conductivity were adopted. The data acquisition procedures described in the following were the same for both the horizontal and the vertical arrangements.

### *2.1.1. Mixing time*

The homogenization process, hence, the mixing time, was investigated by rapidly injecting from the top of the tank in the vicinity of the wall a tracer, that consists of 50 ml of a saturated aqueous solution of NaCl. The measured variable, $C_i$, which is the dimensionless conductivity in cell i, was calculated as the conductivity of the medium during the tracer dispersion divided by the reference conductivity. The reference conductivity was measured before the tracer addition, collecting 500 instantaneous frames after fixing the impeller speed and the gas flow rate selected for the mixing time determination. The conductivity obtained from the average of the 500 instantaneous frames was finally adopted as the reference conductivity. This approach enables decoupling the effect of the dispersion of the gas from the injection of the brine solution on the conductivity distribution. The conductivity of the medium was measured at a frequency of 0.2 frames per second, the acquisition started 15 seconds before the brine addition and was stopped after the achievement of the complete homogenization.

The analysis of the results is based on the normalized local dimensionless conductivity, $\chi_i(t)$, that is defined as:

$$\chi_i(t) = \frac{C_i(t) - C_i(0)}{C_i(\infty) - C_i(0)} \quad (1)$$

Therefore, $\chi_i(0) = 0$ and $\chi_i(\infty) = 1$, irrespective of the initial and final conductivity values. As a result, the plane average of the normalized dimensionless conductivity, $\bar{\chi}$, is a suitable variable for the estimation of the liquid mixing time (Babaei et al., 2015; Paglianti et al., 2017), that is defined as the time required to reach a level of variation within ±(1-x) % of $\bar{\chi}(\infty)$, being x the desired degree of homogeneity. In this work, x is fixed at 0.95, thus determining the so-called $t_{95}$ mixing time. From triplicate measurements, the maximum relative error of the mixing time estimation was found equal to 9%. The mixing dynamics was further observed by the Coefficient of Variation (CoV) of the normalized local dimensionless conductivity calculated as (Paglianti et al., 2017):

$$CoV = \sqrt{\frac{\sum_{i=1}^{N_c} \left(\frac{\chi_i}{\bar{\chi}} - 1\right)^2}{N_c - 1}} \quad (2)$$

Where $N_c$ is equal to the total number of cells for each arrangement, that is equal to 948 and 160 for the horizontal and the vertical measurements, respectively, and $\bar{\chi}$ is the average value of the normalized conductivity over the $N_c$ values.

*2.1.2 Gas hold-up*

For the gas hold-up determination, $C_i$ was obtained as the ratio between the conductivity measured at the selected impeller speeds and gas flow rates under steady state conditions and the reference conductivity. The reference conductivity was obtained from the average of 500 instantaneous frames collected in single phase conditions ($Q_G$=0 L min$^{-1}$) with a very dilute solution of sodium chloride in demineralised water (salt concentration of 0.5 g/L) stirred at the impeller speed at N=50 rpm. The conductivity of the gas-liquid dispersion was obtained from the average of 1500 instantaneous measurements collected at the frequency of 0.2 frames per second.

The local values of the gas hold-up, α, which will be presented in the results, are estimated from the dimensionless conductivity by the application of the well-known Maxwell equation (Khalili et al., 2017) in the case of the non-conducting dispersed phase, as:

$$\alpha_i = \frac{2-2C_i}{C_i+2} \tag{3}$$

Experiments repeated three times led to evaluating the uncertainty of the conductivity measurement, obtaining a maximum relative error on each cross section equal to 0.6%.

The gas hold-up distributions in all planes of measurement (vertical and horizontal) are used to identify and classify the different regimes. The quantitative determination of the transitions between one regime and the other is based on the CoV of the gas hold-up. Similarly to the CoV of the normalized local dimensionless conductivity, the CoV of the gas hold-up is calculated as:

$$CoV = \sqrt{\frac{\sum_{i=1}^{N_c}\left(\frac{\alpha_i}{\bar{\alpha}}-1\right)^2}{N_c-1}} \tag{4}$$

Where $N_c$ is equal to the number of cells on each plane, that is 316 and 160 for the horizontal and the vertical planes, respectively, and $\bar{\alpha}$ is the average value of the gas hold-up over the $N_c$ values on the plane.

The same CoV definition was already adopted to characterize the regime transitions and the dispersed phase distribution in liquid-liquid (Maluta et al., 2020) and solid-liquid (Carletti et al., 2014) systems.

## 3. Results and Discussion

### *3.1 Comparison of results obtained in vertical and horizontal planes*

One of the aims of this work is to evaluate the quantitative validity of the ERT results in order to use them not only for gaining insight into the gas-liquid hydrodynamic characteristics but as a validation tool for modelling results. To this end, the comparison between the radial profiles measured at the $z_1$ and $z_2$ elevations with the horizontal and the vertical electrodes arrangement is reported in Figure 2. The $z_1$ and $z_2$ elevations adopted in the horizontal arrangement were selected, since they coincide with the elevations of the 5th and 13th electrode of the vertical arrangement, being the 1$^{st}$ electrode placed at 180 mm from the vessel bottom. Figures 2a and 2b refer to the flooding condition, while Figures 2c and 2d refer to complete dispersion condition.

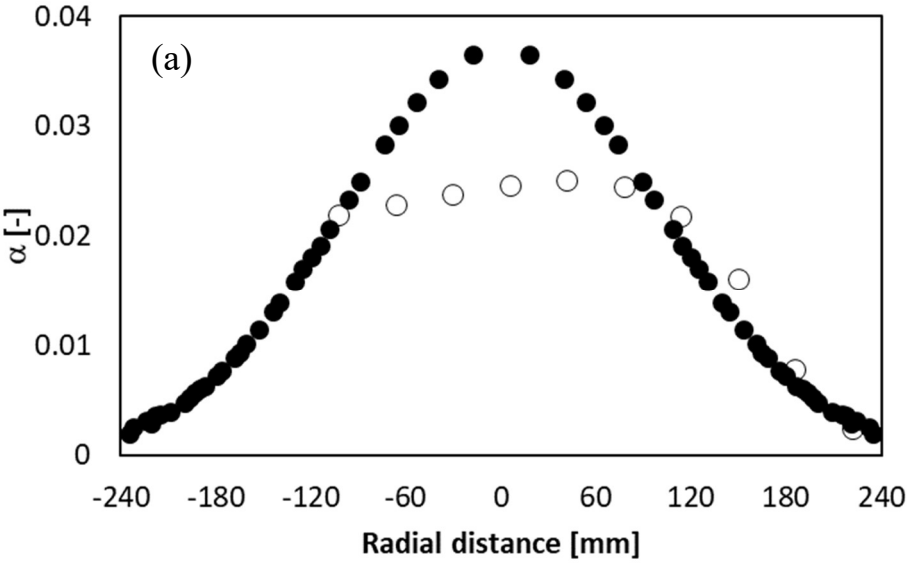
(a)
0.04
0.03
0.02
0.01
0
α [-]
-240
-180
-120
-60
0
60
120
180
240
Radial distance [mm]

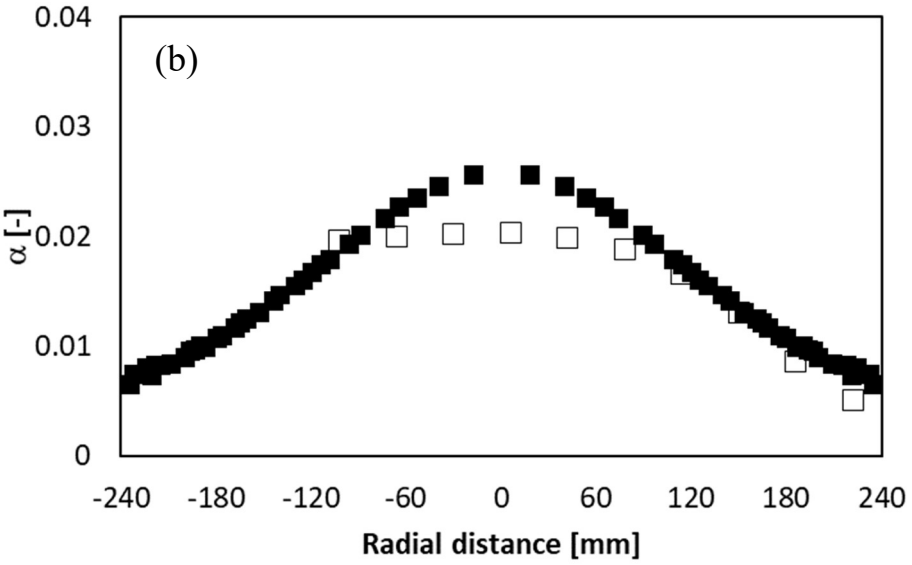
(b)
0.04
0.03
0.02
0.01
0
α [-]
-240
-180
-120
-60
0
60
120
180
240
Radial distance [mm]

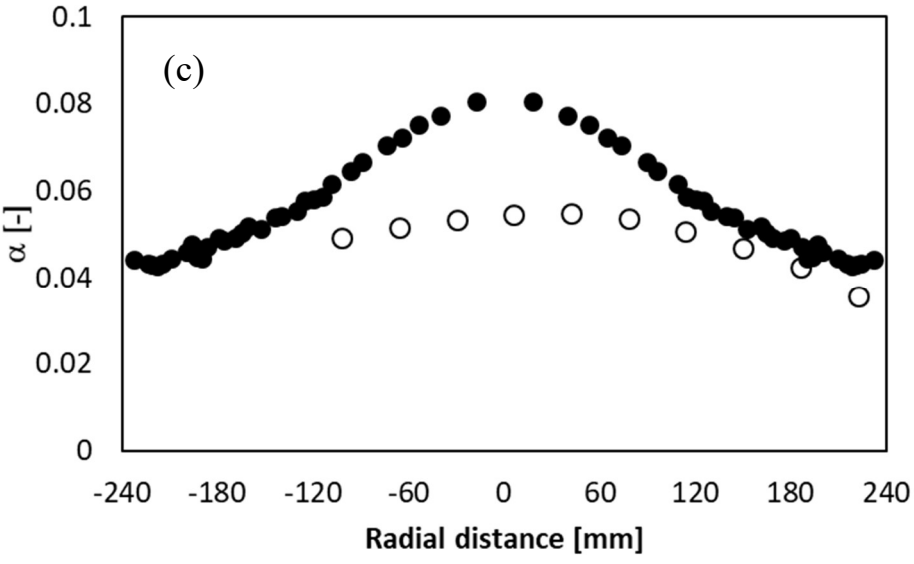
(c)
0.1
0.08
0.06
0.04
0.02
0
α [-]
-240
-180
-120
-60
0
60
120
180
240
Radial distance [mm]

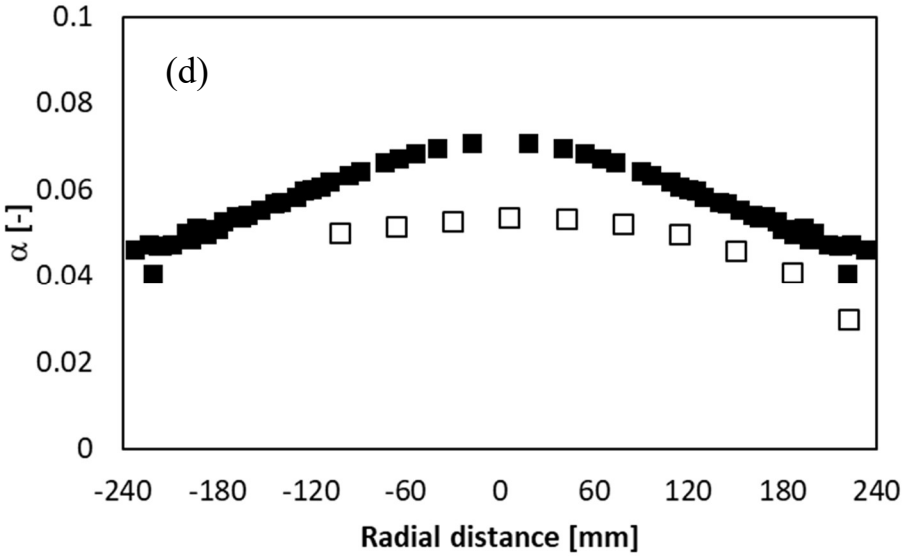


Figure 2 Comparison of radial profiles of averaged gas hold-up obtained with the vertical and the horizontal arrangement of the electrodes. Solid symbols: horizontal arrangement, open symbols: vertical arrangement. (a) N=50rpm, $Q_G$=50 L/min, $z_1$; (b) N=50rpm, $Q_G$=50 L/min, $z_2$; (c) N=500rpm, $Q_G$=50 L/min, $z_1$; (d) N=500rpm, $Q_G$=50 L/min, $z_2$.

As can be observed, the qualitative trend obtained with the two arrangements is similar, being in both cases at the centre of the tank (r=0 mm) the gas hold-up greater than close to the wall where the vertical electrodes are located (r=240 mm). As expected, moving from flooding to complete dispersion condition, at a constant gas flow rate, the measured gas hold-up increases both with the vertical and the horizontal arrangement of the electrodes.

On a quantitative basis instead, the measured values are not coincident, the vertical measurements match quite well the horizontal ones close to the electrodes, but the agreement decreases moving far from the electrodes and worsens closer to the centre of the tank. From a preliminary evaluation, although the higher resolution is obtained in the axial direction (Forte et al., 2019), the accuracy of the horizontal arrangement is higher with respect to the vertical one in the central region of the tank, since with the adjacent strategy and the horizontal arrangement the voltage difference across the entire section is measured by two opposite electrodes, while with the vertical arrangement the voltage difference is measured by the electrodes placed on the same side.

The accuracy of the gas hold-up measurements obtained with the two arrangements is estimated by the comparison with the overall gas hold-up obtained by measuring the increment of the liquid level with respect to single phase conditions. The results shown in Figure 3 confirm that

with the vertical arrangement the values are generally smaller than those obtained with the horizontal arrangement. At the lower impeller speeds, the agreement between the overall gas hold-up estimated with the two methods is satisfactory. The agreement worsens at increasing gas flow rate, due to the inhomogeneous gas distribution in the vessel volume, which limits the significance of the comparison between the overall gas hold-up and the hold-up on the plane.

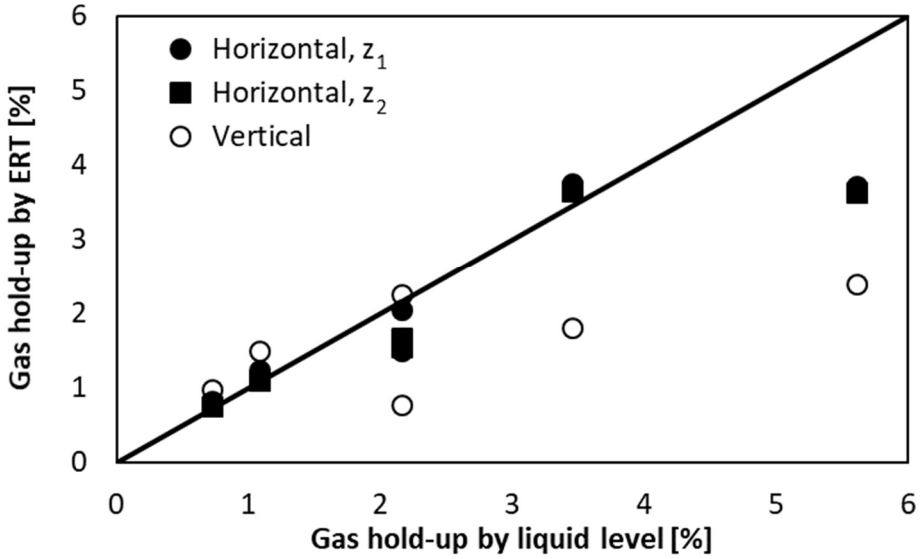


Figure 3. Comparison of average gas hold-up obtained by ERT on the vertical and the horizontal planes, and the overall gas hold-up estimated from the increment of the liquid level. Solid symbols: horizontal arrangement, open symbols: vertical arrangement.

The plane averaged tracer homogenization dynamics obtained with the two types of ERT measurements (vertical vs horizontal) are shown in Figure 4 for one ungassed (Figure 4a) and two gassed conditions (Figures 4b and 4c). Specifically, the time traces of the Coefficient of Variation of the normalized local dimensionless conductivity, $\chi_i(t)$, for the horizontal and the vertical arrangements of the electrodes are compared. The curves relevant to the horizontal arrangement are obtained from the average of the results on the three planes.

The experimental data shown in Figure 4 clearly demonstrate that with the horizontal and the vertical arrangements the same trend of the mixing dynamics is observed.

In the particular operating condition considered in Figure 4, the gas phase enhances the liquid mixing leading to a shorter mixing time with respect to the single-phase condition at the same impeller speed, as it is possible to notice comparing the results reported in Figures 4 (a) and 4

(b). At equal gas flow rate, the effect of the impeller speed appears less relevant, as can be noticed by comparing the results shown in Figures 4 (b) and 4 (c).

It is worthwhile noticing that the numerical evaluation of the mixing time by using the CoV analysis is possible for the loading and the complete recirculation regime, while it is not possible in the flooding regime because, as shown in Figure 4 (b), the presence of large bubbles induces wide oscillations of the asymptotic value. For this reason, in the following, the quantitative analysis of the mixing time results will be performed considering the time traces of the plane averaged normalized dimensionless conductivity, which is suitable for the quantitative determination at any flow regime.

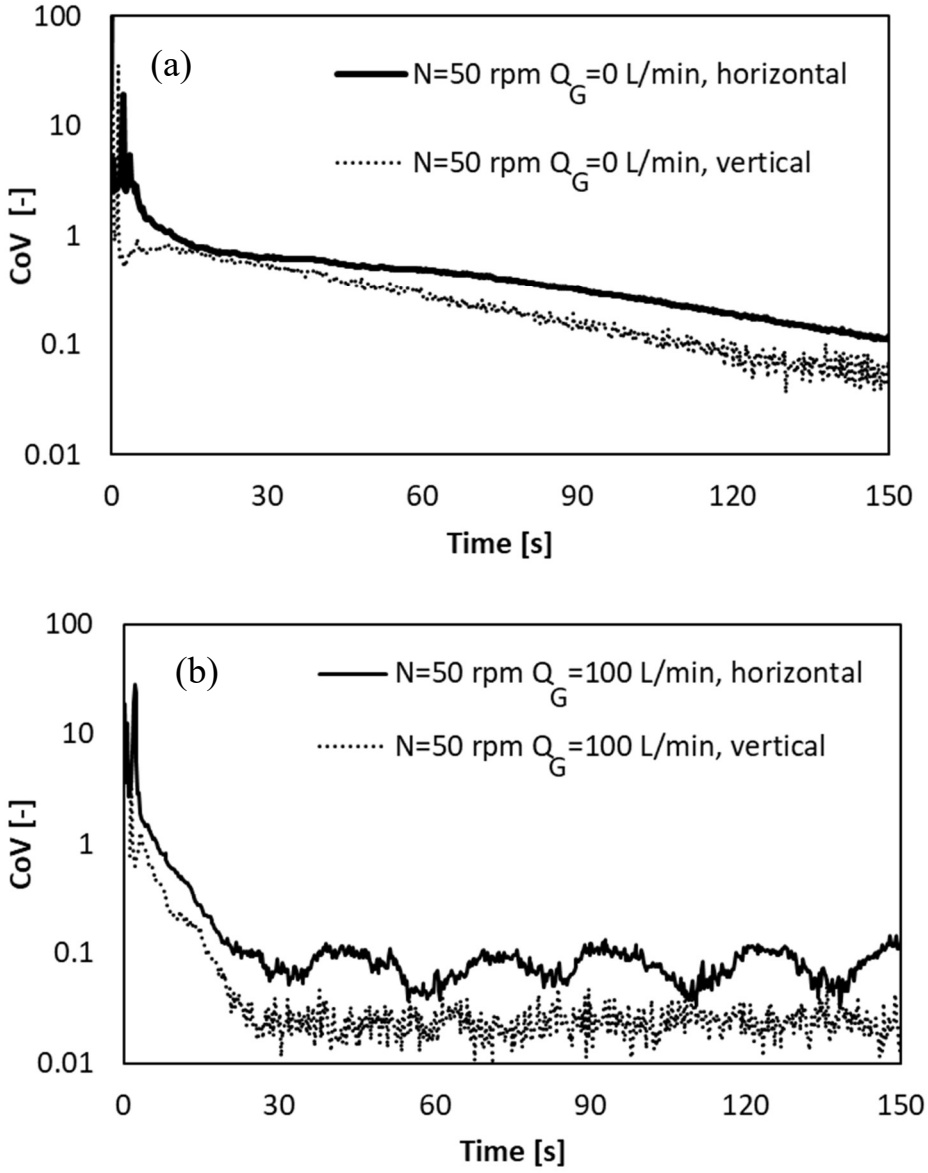

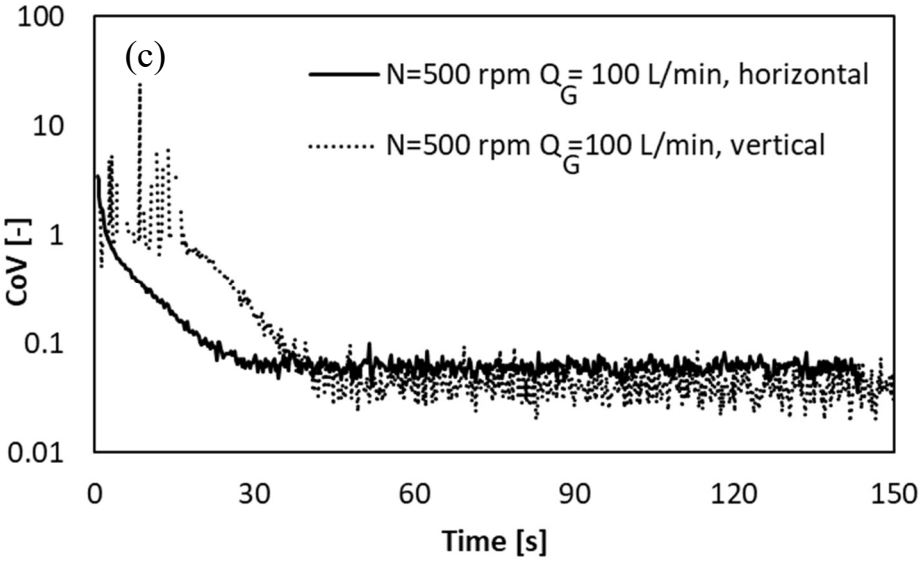


Figure 4 Time traces of the Coefficient of Variation of $\chi_i(t)$ obtained the vertical and the horizontal arrangement of the electrodes. (a) N=50rpm, $Q_G$=0 L/min; (b) N=50rpm, $Q_G$=100 L/min; (c) N=500rpm, $Q_G$=100 L/min.

*3.2 Gas hold-up distributions*

The determination of the gas hold-up distribution in the vessel volume is extremely useful for the quantitative detection of the flow regime occurring in the equipment, which depends on the specific combination of N and $Q_G$ and is often obtained by visual observations. When the lowest impeller is not able to disperse the gas in the tank, the gas flows upward in the centre, the liquid in the rest of the tank is practically ungassed and, in this case, the flow regime is called flooding. Increasing N, the mechanical power transferred by the impeller to the mixture allows to disperse the gas bubbles mainly above the impeller, but it is not sufficient to induce a recirculation of the gas-phase below the lowest impeller and the flow regime is called loading. If the impeller speed is further increased, the gas-phase is dispersed in the whole vessel volume, in this case the regime is called complete recirculation. From the industrial production point of view, the identification of the flow regime is of primary importance, because if the stirred tank works in the flooding conditions, the efficiency of the mass transfer process drops dramatically (Noorman et al., 2018; Maluta et al., 2022).

In the first part of this work, both the vertical and horizontal planes have been used to classify the different regimes. Examples of the gas hold-up distributions in the vertical and in the lower horizontal measurement planes are shown in Figure 5. The lower part of vertical plane and the

$z_1$ horizontal plane have been selected to show clearly the different regimes according to the distribution of hold-up.

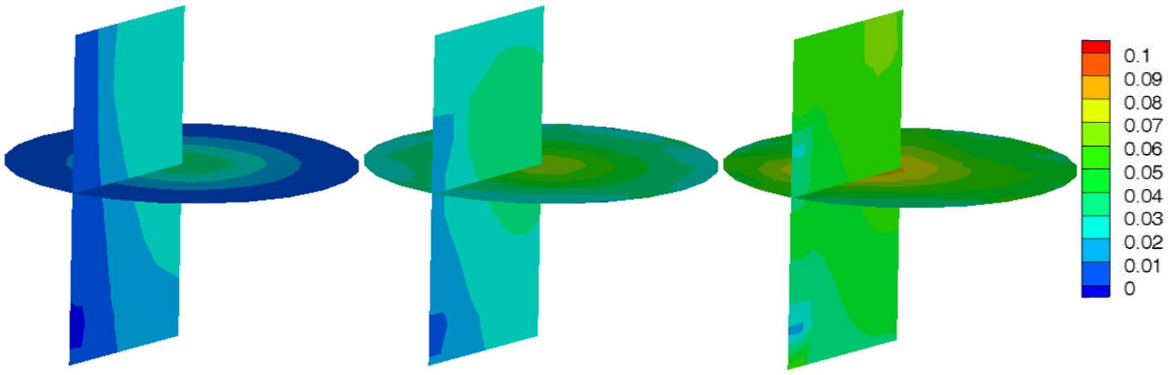


(a) (b) (c)

Figure 5 Gas hold-up on the vertical (area between bottom of the tank and $z_2$ plane) and the horizontal $z_1$ planes, $Q_G$ = 50L/min. (a) N=50rpm (b) N=200rpm; (c) N=500rpm.

In Figure 5 (a) the flooding condition is apparent since the gas phase flows in the centre of the tank and the turbine is not able to disperse it. In Figure 5 (b) the loading condition is shown, since in the lower part of the tank the gas phase is present only in the centre of the tank, because of the sparger presence, but the impeller cannot induce the recirculation of the gas-phase. Finally, in Figure 5 (c) the complete recirculation condition can be observed, corresponding to gas distribution both below and above the lowest impeller. The results demonstrate that this local analysis allows to detect the different regimes, confirming previous results obtained with a linear probe in a single impeller stirred tank (Forte et al., 2019).

In Figure 6, the CoV values estimated on the $z_1$ plane clearly show that the flooding regime corresponds to significantly greater values of CoV than those measured in the loading and complete recirculation regimes, revealing larger hold-up gradients and a subsequent lower homogeneity on the plane.

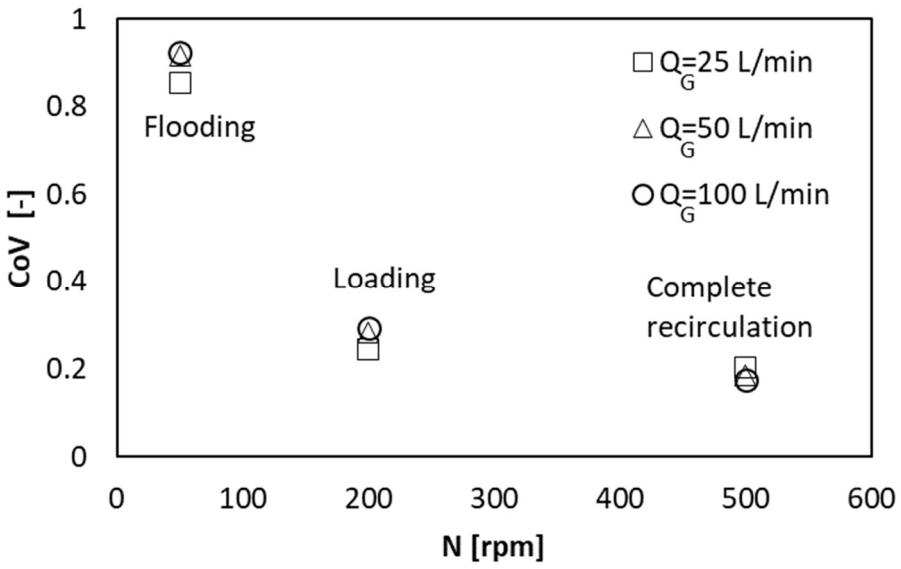


Figure 6 CoV of the gas hold-up estimated on $z_1$.

A quantitative evaluation of the working condition effects on the gas hold-up distribution can also be obtained by the comparison of the radial profiles of gas hold-up averaged on the azimuthal coordinate at fixed elevations, as shown in Figure 7.

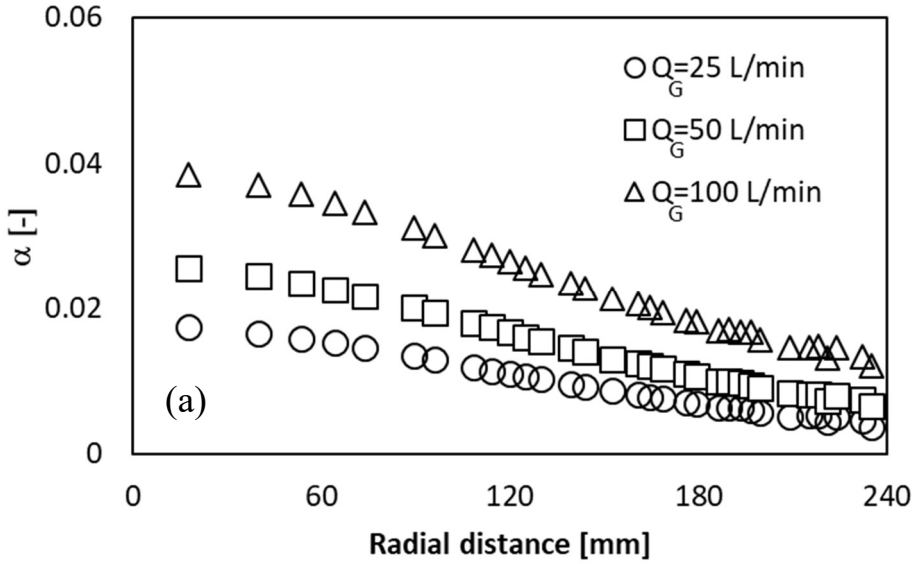

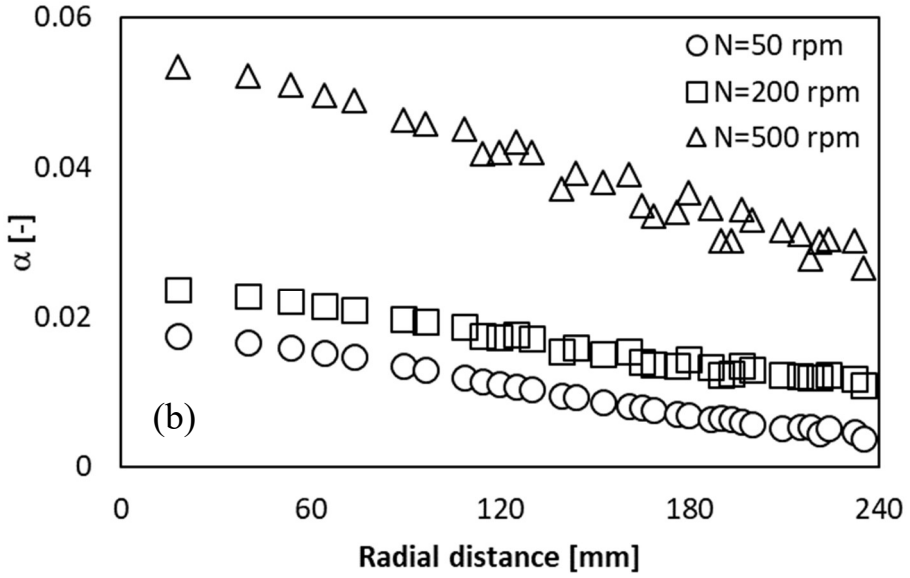


Figure 7 Radial profiles of averaged gas hold-up on $z_2$. (a) Effect of $Q_G$ at N=50 rpm; (b) Effect of N at $Q_G$=25 L/min.

The gas hold-up exhibits an increase at increasing gas flow rate and impeller speed and higher values towards the centre (radial distance, r, equal to 0) with respect to the vessel wall (r=240 mm). The profiles can provide a quantitative benchmark for modelling strategies, which are of crucial importance for improving the scale-up of gas-liquid stirred (bio-)reactors (Maluta et al., 2021).

*3.3 Liquid homogenization dynamics*

The time traces of the normalized conductivity averaged on each plane for the case of the horizontal and vertical configurations are shown in Figure 8, either in single phase (Figure 8 (a)) or in two-phase (Figure 8 (b)) conditions at the same impeller speed. In both cases, the acquisition started 15 seconds before the injection of the concentrated solution, identified as the time, t, equal to zero.

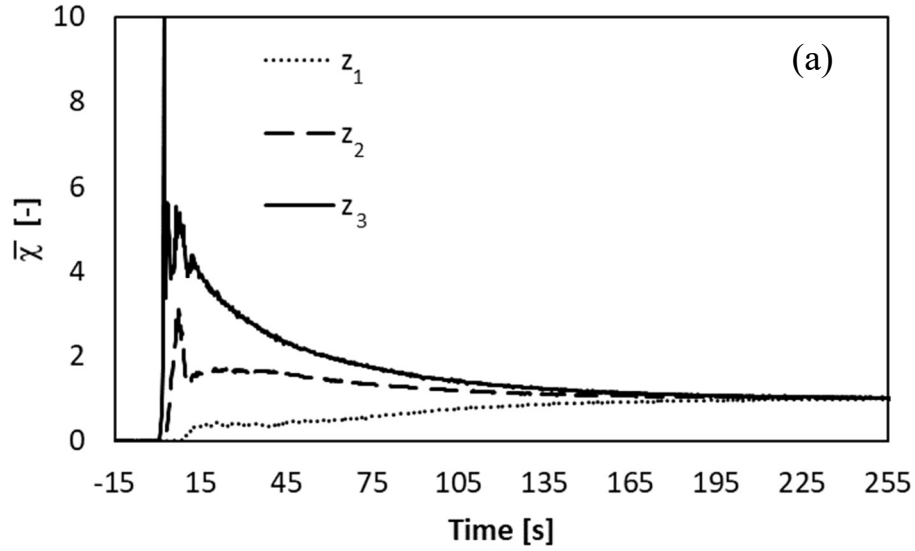
(a)
z1
z2
z3
χ̄ [-]
Time [s]

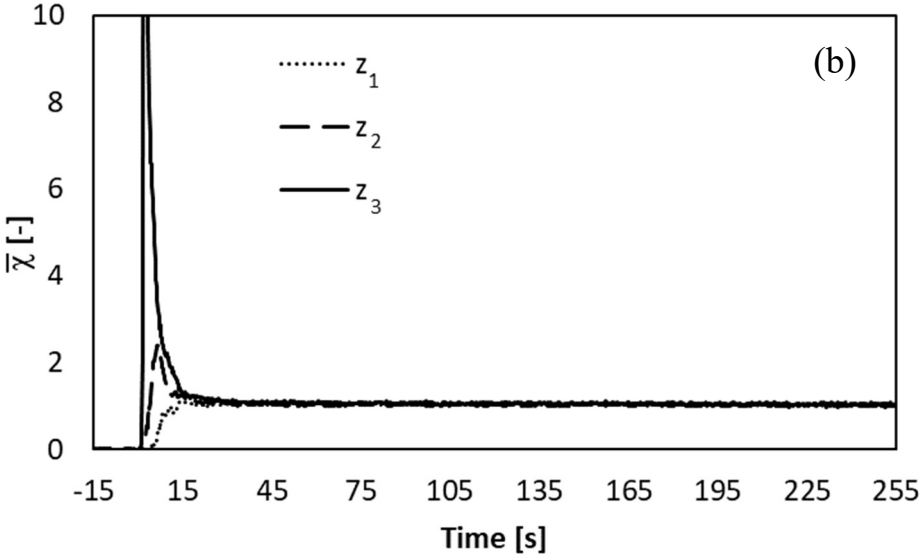
(b)
z1
z2
z3
χ̄ [-]
Time [s]

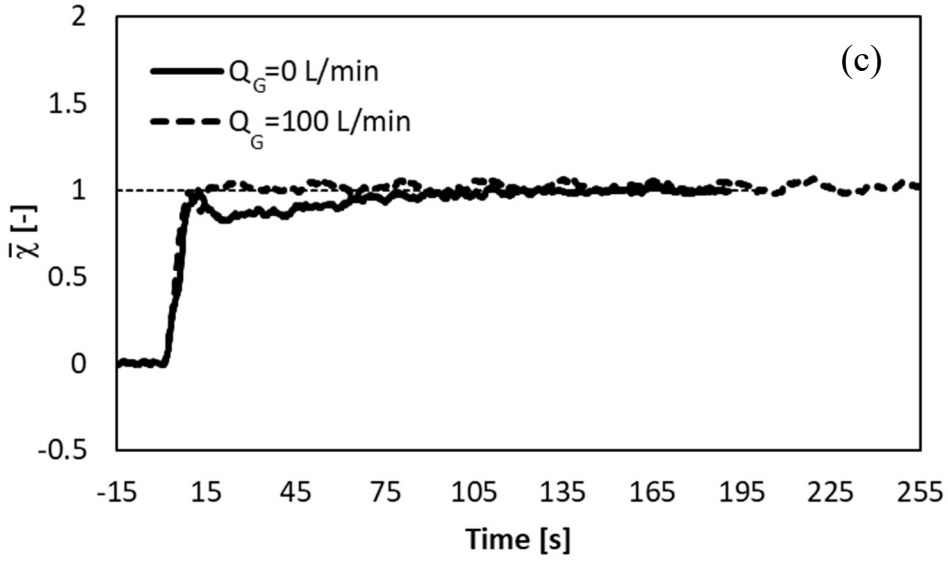
(c)
QG=0 L/min
QG=100 L/min
χ̄ [-]
Time [s]

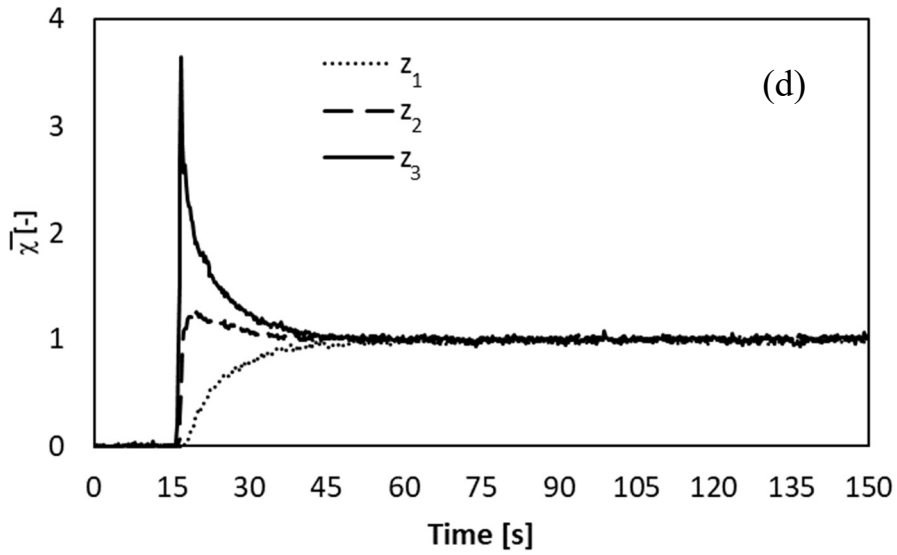


Figure 8 Time trace of $\bar{\chi}$ . Horizontal planes: (a) N = 50 rpm $Q_G$ = 0 L/min, (b) N = 50 rpm $Q_G$=100 L/min. Vertical plane: (c) N = 50 rpm for $Q_G$ = 0 L/min and $Q_G$ = 100 L/min. Horizontal planes: (d) N = 500 rpm $Q_G$=100 L/min.

As can be observed from the comparison between the Figures 8 (a) and 8 (b), the action of the gas bubbles in the system significantly reduces the time necessary for the liquid homogenization on the three horizontal measurement planes, being the mixing time in single phase conditions (Figure 8 a) one order of magnitude longer than that measured in the gassed system (Figure 8 b), at the same impeller speed. The same conclusion is drawn from the comparison of the time traces obtained with the vertical arrangement, shown in Figure 8 (c). The effects of the flow regime changing from flooding (Figure 8 b) to complete dispersion regime (Figure 8 d), are less marked than those induced by the presence of the gas phase with respect to the single phase.

The effect of the dispersed phase on the characteristic mixing time can be clearly explained from the observation of the local values of the normalized dimensionless conductivity, shown in Figures 9 (a) and (b), relevant to the results in the single-phase and in the two-phase system, respectively at different times, with the tracer injection corresponding to t=0 s.

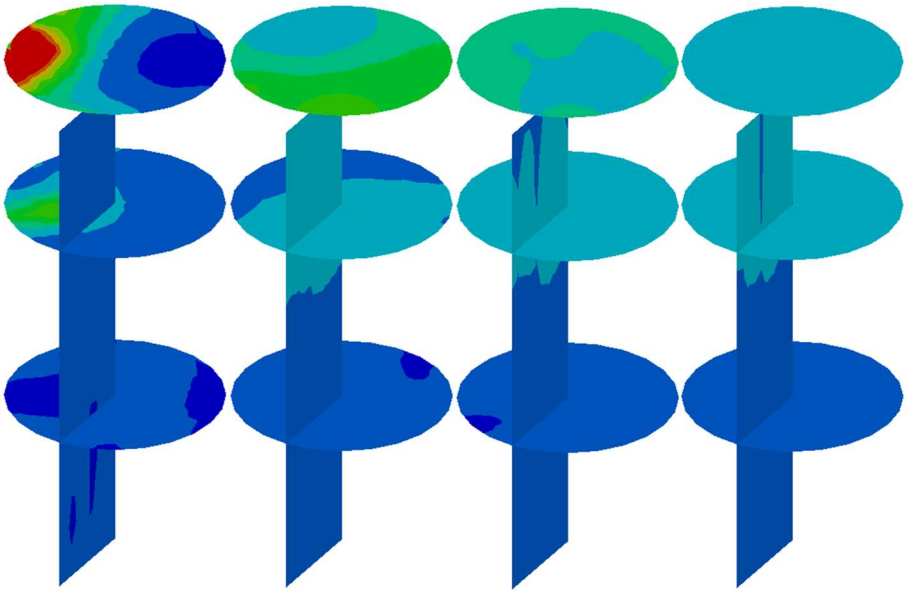


(a)

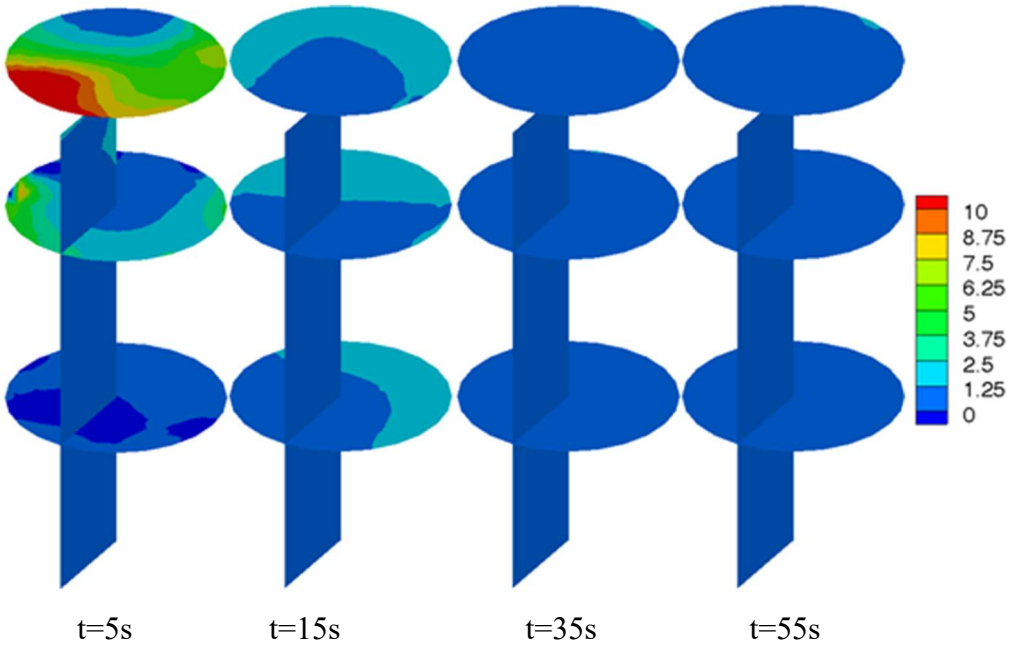


(b)

Figure 9 Snapshots of $\chi_i$ on the measurement planes. N = 50 rpm, (a) $Q_G$ = 0 L/min. (b) $Q_G$ = 100L/min.

The comparison between the results in Figures 9 (a) and (b) shows the reason for the longer homogenization time in the single phase with respect to the gas-liquid system, observed in Figure 8. As found in previous investigations (Rodgers et al., 2011), in the single-phase case

(Figure 9 (a)) a zoning effect is apparent from the high conductivity measured for a long time in the upper part of the tank. It confirms that the mass exchange between adjacent impellers in the case of multiple radial turbines with the adopted spacing is not very efficient (Magelli et al., 2013). At the investigated impeller speed, the presence of the gas phase increases the mass transfer between two adjacent impellers cancelling the zoning behaviour (Figure 9 (b)). It is worth observing that depending on the geometrical configuration and the working conditions of the stirred tank, the gas phase can lead to the opposite effect, as recently observed by Jamshed et al. (2019). The advantage of the ERT technique with respect to pointwise methods is clearly to provide local and whole-field information on the homogenization dynamics (Carletti et al., 2016), thus leading to a clear interpretation of the mixing time values. An additional example of the usefulness of simultaneous estimation of the mixing time obtained from the plane average of the normalized dimensionless conductivity on different vessel sections for all the flow regimes taking place in the stirred tank, is provided in Figure 10. The mixing times measured at different gas flow rates and impeller speeds in the upper ($z_3$=1260 mm), and the lower ($z_1$=420 mm) horizontal measurement planes are compared.

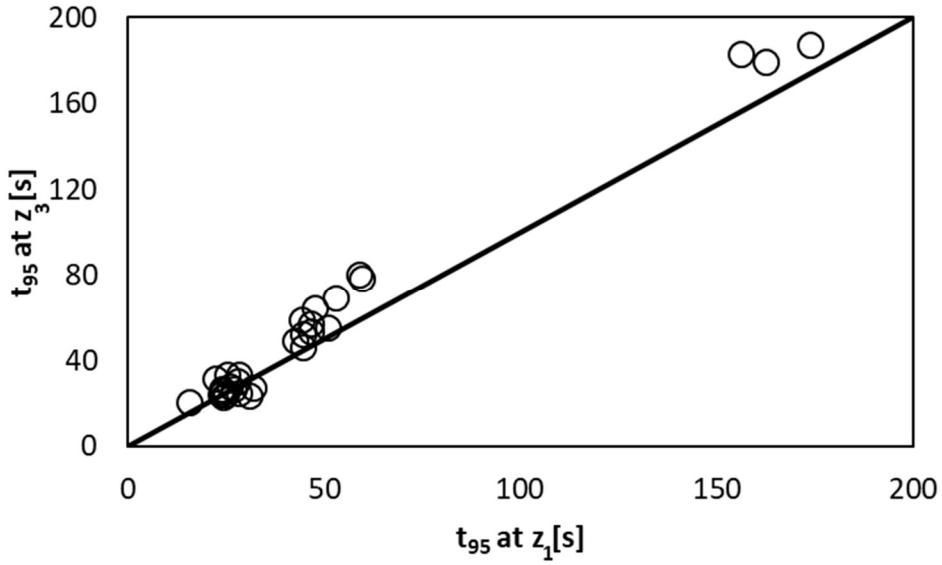


Figure 10 Deviation of $t_{95}$ values estimated at different elevations. $Q_G$ = 0- 200 L/min N= 50-500 rpm.

A mean difference in the mixing time value of 14% is found in the investigated conditions, confirming that the characteristic time necessary for reaching the homogeneous conditions can be different depending on the measurement location. In the following, the analysis is based on

the mixing time estimated in the upper plane, which is the slowest to achieve homogenous conditions.

The effect of the operative conditions on $t_{95}$ is shown in Figure 11. The results evidence the effects of the complex fluid dynamics interactions occurring in multiple impeller stirred tanks both in single phase and in gas-liquid conditions. The highest value of mixing time is measured in the single phase condition at low impeller speed. As expected, by increasing the impeller speed a reduction of the mixing time in the ungassed liquid is obtained. The high value of the measured mixing time is due to the zoning effect pointed out, among others, by Magelli et al. (2013). This behaviour is particularly relevant at the lowest impeller speed (N=50 rpm), where a significant reduction of the mixing time can be observed moving from single phase to two-phase systems, while a weak effect of the gas phase is observed at higher impeller speeds. Increasing the gas flow rate from 25 L/min up to 100 L/min, the mixing time weakly changes with N. This experimental behaviour has been also noted by Vrâbel et al. (1999) in stirred tanks equipped with multiple Rushton turbines using fluorescent tracer and optical probes.

Another interesting experimental result is that under aeration, at N=200 rpm, longer mixing times are observed with respect to those measured at 50 rpm. this is not a trivial outcome that is probably due to a particular gas-liquid flow pattern that establishes in the stirred tank. In fact, depending on the working conditions, increasing the impeller speed may increase the time necessary for the homogenization of a reactant. In the following, the analysis of the local conductivity measurements is performed to gain insight into the complex effects induced by the impeller speed and the gas flow rate.

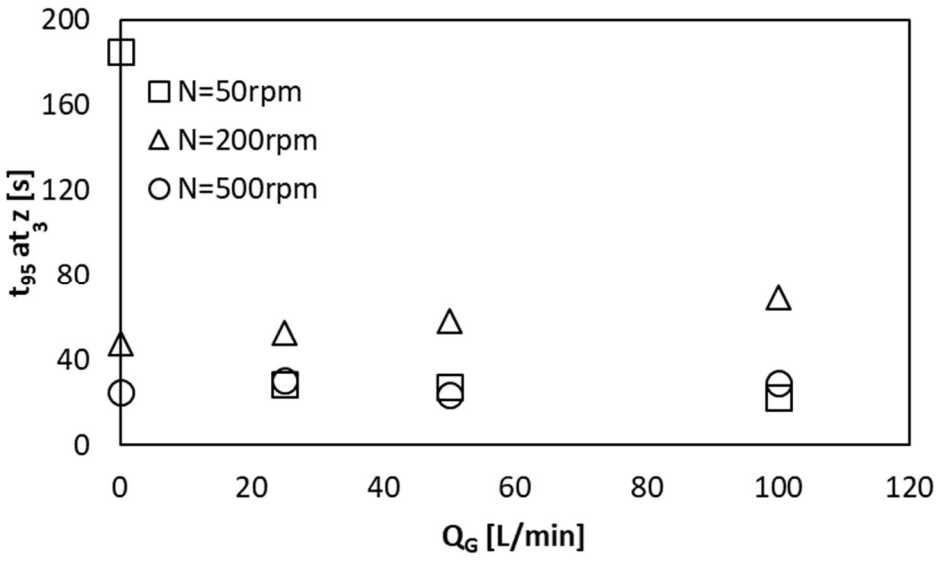


Figure 11. Effect of working conditions on $t_{95}$.

The dimensionless conductivity maps on the horizontal planes allow to appreciate the different flow patterns induced by the gas phase, following the dispersion of the high conductivity mixture during the mixing time experiments. As an example, a few snapshots of the dimensionless conductivity maps in the first ten seconds after the tracer injection in the single phase and in the gas-liquid systems are shown in Figure 12 (a) and (b), respectively. Focusing on the upper plane, it can be noticed that, in single phase flow (Figure 12 (a)), the high conductivity mixture goes from the upper to the middle plane moving from the vessel wall to the centre of the upper plane and then to the centre of the middle plane (red lines). In the two-phase case (Figure 12 (b)), the gas flows preferentially in the centre of the tank inducing a movement of the liquid phase that is directed upward in the centre of the tank and downward close to the wall (blue lines). Therefore, the high conductivity mixture, which is injected close to the wall of the upper surface, goes from the upper to the middle plane moving close to the vessel wall (red lines). Also, a motivation for the higher value of $t_{95}$ obtained at N=200 rpm can be found from the analysis of the snapshots recorded at the beginning of the mixing time experiments at different impeller speeds.

The comparison between the results shown in Figure 13 (a,b,c), Figure 13 (d,e,f) and Figure 13 (g,h,i) collected at N=50rpm, N=200rpm and N=500rpm respectively highlight that the possible reason for the increment of $t_{95}$, at N=200 rpm, shown in Figure 11 can be associated to the opposite flows induced by the impeller and the gas phase in the upper part of the tank, reported on the right of the Figures 12 (a) and (b).

When the gas action prevails over the action of the impeller, the high conductivity mixture added on the top of the stirred tank is practically homogenized in less than 35 seconds, as shown in Figure 13 (b). When N is equal to 200 rpm the two effects, acting in opposite ways, are partially balanced and the high conductivity mixture remains unmixed in the upper part of the vessel for more than 35 seconds, as shown in Figure 13 (e, f). When the action of the impeller prevails on the gas action, the upper part of the tank is homogenized in less than 35 seconds, as shown in Figure 13 (h, i).

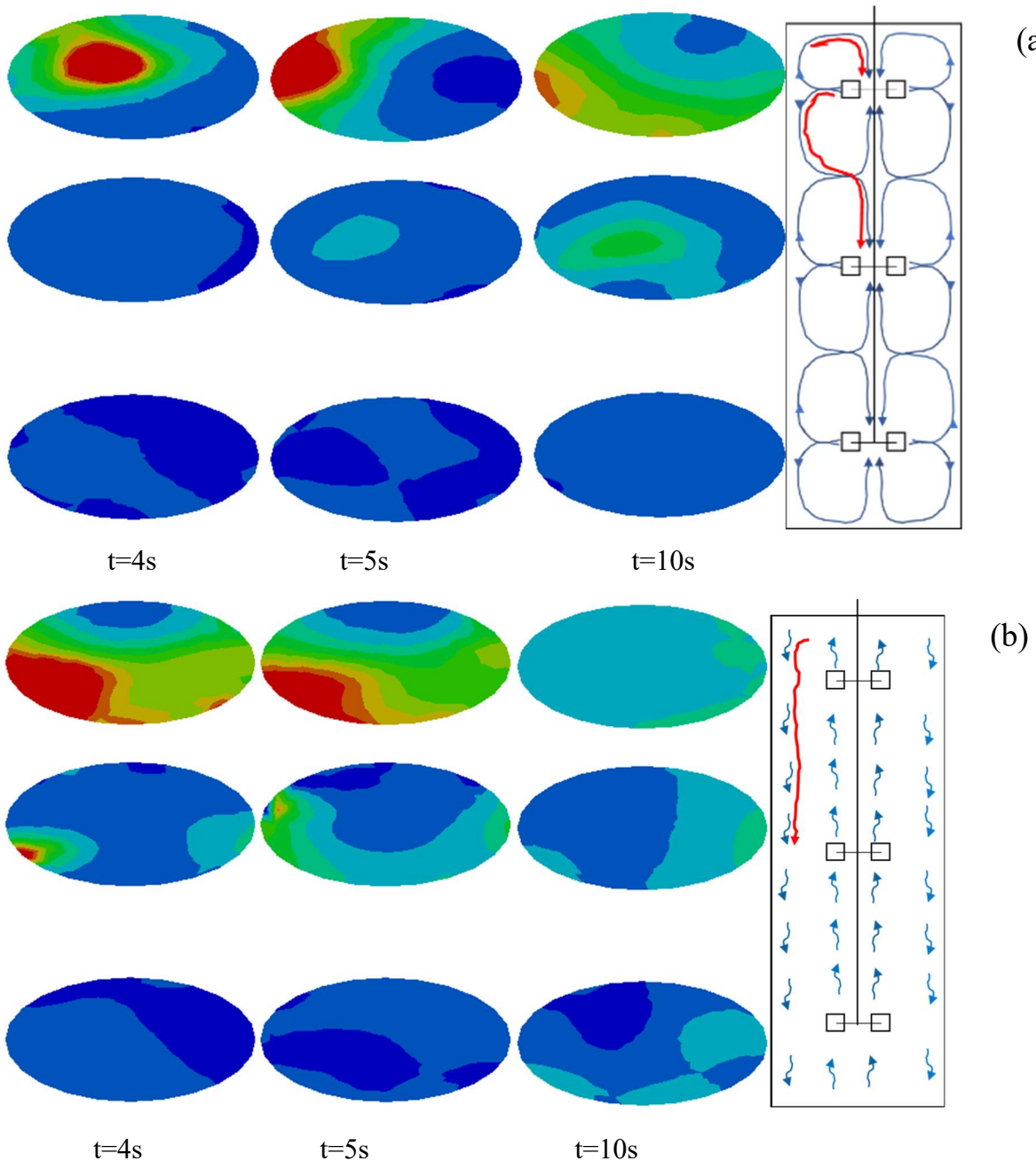


Figure 12 Snapshots of $\chi_i$. N = 50 rpm (a) $Q_G$ = 0L/min, (b) $Q_G$ = 100L/min Colour scale as in Figure 9.

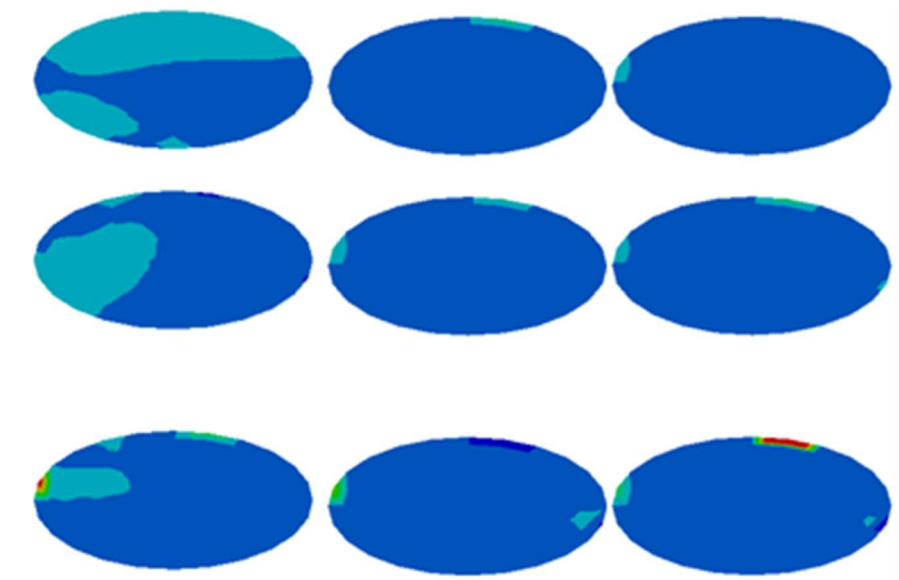

(a) (b) (c)

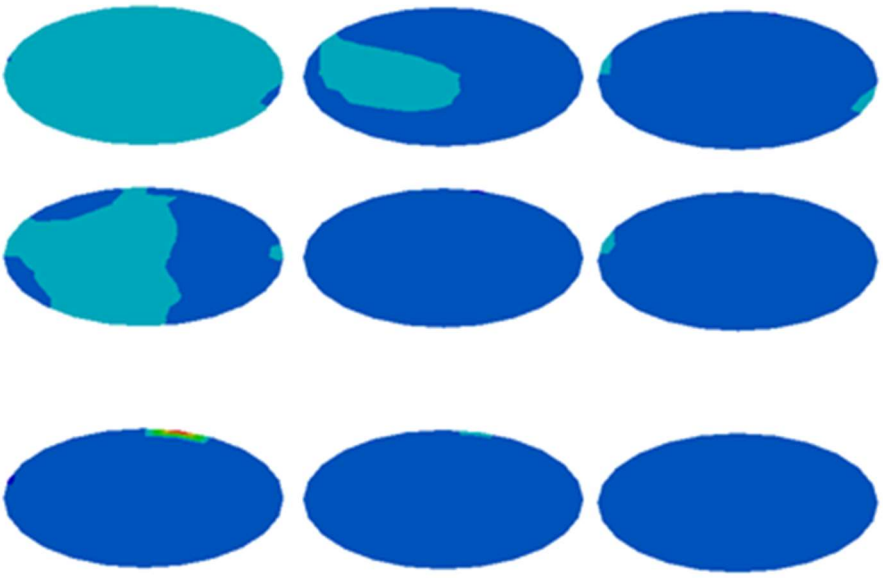

(d) (e) (f)

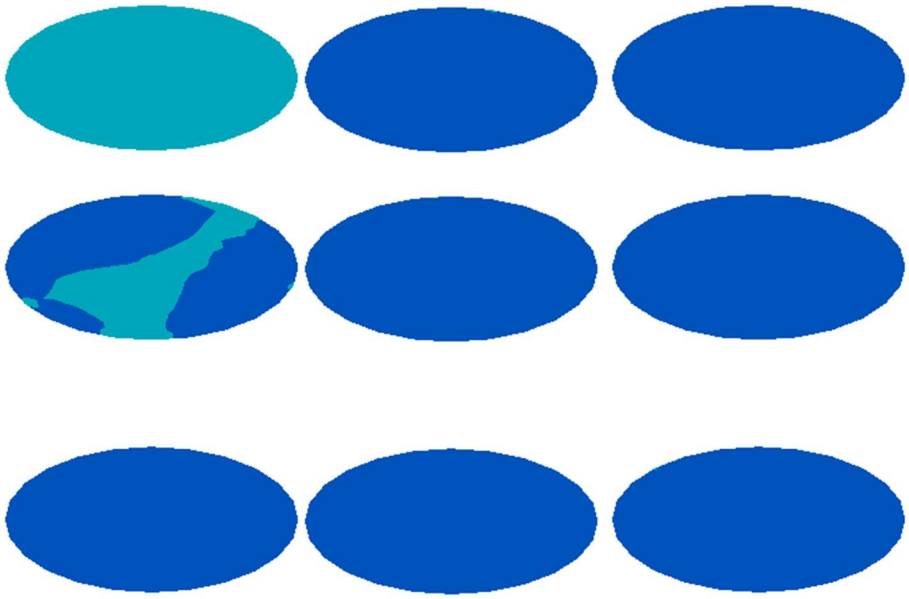

(g) (h) (i)

Figure 13 Snapshots of $\chi_i$. N = 50 rpm, $Q_G$ = 25L/min. (a) t=15s; (b) t=35s, (c) t=55s; N = 200 rpm, $Q_G$ = 25L/min. (d) t=15s; (e) t=35s, (f) t=55s; N = 500 rpm, $Q_G$ = 25L/min. (g) t=15s; (h) t=35s, (i) t=55s. Colour scale as in Figure 9.

## 4. Conclusions

ETR data have been collected and analysed for the determination of liquid mixing time, gas-liquid flow regimes and gas hold-up distributions in a multiple impeller pilot stirred tank of geometry similar to that of widespread stirred tank bioreactors adopted for industrial aerobic fermentations. Vertical and horizontal arrangements of the electrodes have been adopted and the analysis of the conductivity data has provided realistic qualitative and quantitative information on the two-phase fluid dynamics and mixing characteristics, as a function of the operative conditions of the stirred tank. The major findings of this study are:

- The gas hold-up distributions obtained with the vertical and horizontal arrangements of the electrodes at the same location are practically coincident close to the vessel wall, while underestimated values are obtained in the vessel central region with the vertical configuration.
- The mixing dynamics curves obtained with the vertical and the horizontal planes provide a similar qualitative trend. For a quantitative estimation of the mixing time

under gassed conditions and all the flow regimes, the plane averaged time trace of the normalized dimensionless conductivity provides the most reliable results.

- The flow regime transition is effectively determined by observing the plane averaged CoV of the gas hold-up on the horizontal plane located below the lower impeller.
- Both arrangements of the electrodes confirm that in multiple impeller systems the presence of the gas phase can cancel the zoning effects.
- The combined information obtained in the vertical (zoning due to multiple impellers) and horizontal planes (plume evolution after tracer injection) allow a sound interpretation of the effect of agitation and gas flow rate on the mixing dynamics.

**Nomenclature**

| | |
|---|---|
| $C$ | impeller clearance, m |
| $C_i$ | dimensionless conductivity in the cell i, dimensionless |
| $C_S$ | sparger clearance, m |
| CoV | coefficient of variation, dimensionless |
| $D$ | impeller diameter, m |
| $D_S$ | sparger diameter, m |
| $H$ | vessel height, m |
| $H_L$ | liquid height, m |
| $N$ | impeller speed, rpm |
| $N_C$ | number of cells, dimensionless |
| $Q_G$ | gas flowrate, L/min |
| $r$ | radial distance, m |
| $T$ | vessel diameter, m |
| $t$ | time, s |
| $t_{95}$ | mixing time at 95% homogeneity level, s |
| $z_1$,$z_2$,$z_3$ | elevation of measurement plane, m |
| $x$ | degree of homogeneity, dimensionless |
| $W$ | baffles width, m |

***Greek letters***

| | |
|---|---|
| $\alpha_i$ | local gas hold-up, dimensionless |
| $\bar{\alpha}$ | plane average gas hold-up, dimensionless |

$\chi_i$ normalized local dimensionless conductivity, dimensionless

$\bar{\chi}$ plane average normalized dimensionless conductivity, dimensionless

## References


Abdullah, B., Adesina, A.A., 2017. Evaluation of gas–liquid mass transfer in gas-induced stirred tank reactor using electrical resistance tomography. J. Chem. Technol. Biot. 92 (8), 2123-2133. https://doi.org/10.1002/jctb.5220.

Babaei, R., Bonakdarpour, B., Ein-Mozaffari, F., 2015. Analysis of gas phase characteristics and mixing performance in an activated sludge bioreactor using electrical resistance tomography. Chem. Eng. J. 279, 874-884. https://doi.org/10.1016/j.cej.2015.05.072.

Cappello, V., Plais, C., Vial, C., Augier, F., 2021. Scale-up of aerated bioreactors: CFD validation and application to the enzyme production by Trichoderma reesei. Chem. Eng. Sci. 229, 116033. https://doi.org/10.1016/j.ces.2020.116033.

Carletti, C., Montante, G., Westerlund, T., Paglianti A. 2014. Analysis of solid concentration distribution in dense solid–liquid stirred tanks by electrical resistance tomography. Chem. Eng. Sci., 119, 53-64. https://doi.org/10.1016/j.ces.2014.07.049.

Carletti, C., Montante, G., De Blasio, C., Paglianti, A., 2016. Liquid mixing dynamics in slurry stirred tanks based on electrical resistance tomography. Chem. Eng. Sci. 152, 478-487. https://doi.org/10.1016/j.ces.2016.06.044.

Deng, X., Dong, F., Xu, L.J., Liu, X.P., Xu, L.A., 2001. The design of a dual-plane ERT system for cross correlation measurement of bubbly gas/liquid pipe flow. Meas. Sci. Technol. 12 (8), 1024-1031. https://doi.org/10.1088/0957-0233/12/8/306.

Ford, J.J., Heindel, T.J., Jensen, T.C., Drake, J.B., 2008. X-ray computed tomography of a gas-sparged stirred-tank reactor. Chem. Eng. Sci. 63 (8), 2075-2085. https://doi.org/10.1016/j.ces.2008.01.007.

Forte, G., Alberini, F., Simmons. M.J.H., Stitt, H. E., 2019. Measuring gas hold-up in gas–liquid/gas–solid–liquid stirred tanks with an electrical resistance tomography linear probe. AIChE J. 65(6), e16586. https://doi.org/10.1002/aic.16586.

Forte, G., Alberini, F., Simmons, M., Stitt, H. E., 2021. Use of acoustic emission in combination with machine learning: monitoring of gas–liquid mixing in stirred tanks. J. Intell. Manuf. 32(2), 633-647. https://doi.org/10.1007/s10845-020-01611-z.

Hashemi, N., Ein-Mozaffari, F., Upreti, S.R., Hwang, D.K., 2016. Experimental investigation of the bubble behavior in an aerated coaxial mixing vessel through electrical resistance tomography (ERT). Chem. Eng. J., 289, 402-412. https://doi.org/10.1016/j.cej.2015.12.077.

Humbird, D., Davis, R., McMillan, J.D., 2017. Aeration costs in stirred-tank and bubble column bioreactors. Biochem. Eng. J. 127, 161-166. https://doi.org/10.1016/j.bej.2017.08.006.

Jamshed, A., Cooke, M., Rodgers, T.L., 2019. Effect of zoning on mixing and mass transfer in dual agitated gassed vessels. Chem. Eng. Res. Des. 142, 237-244. https://doi.org/10.1016/j.cherd.2018.12.011.

Jamshidzadeh, M., Ein-Mozaffari, F., Lohi, A., 2021. Local Distribution of Oxygen Mass Transfer Coefficient in CMC Solutions in Bioreactors Furnished with Different Types of Coaxial Mixers. Chem. Eng. Res. Des. 174, 213-224. https://doi.org/10.1016/j.cherd.2021.08.006.

Khalili, F., Jafari Nasr, M.R., Kazemzadeh, A., Ein-Mozaffari, F., 2017. Hydrodynamic performance of the ASI impeller in an aerated bioreactor containing the biopolymer solution through tomography and CFD. Chem. Eng. Res. Des. 125, 190-203. https://doi.org/10.1016/j.cherd.2017.07.016.

Magelli, F., Montante, G., Pinelli, D., Paglianti, A., 2013. Mixing time in high aspect ratio vessels stirred with multiple impellers. Chem. Eng. Sci. 101, 712-720. https://doi.org/10.1016/j.ces.2013.07.022.

Maluta, F., Montante, G., Paglianti, A., 2020 Analysis of immiscible liquid-liquid mixing in stirred tanks by Electrical Resistance Tomography. Chem. Eng. Sci. 227, 115898. https://doi.org/10.1016/j.ces.2020.115898

Maluta, F., Paglianti, A., Montante, G., 2021. Two-fluids RANS predictions of gas cavities, power consumption, mixing time and oxygen transfer rate in an aerated fermenter scale-down stirred with multiple impellers. Biochem. Eng. J. 166, 107867. https://doi.org/10.1016/j.bej.2020.107867.

Maluta, F., Paglianti, A., Montante, G. 2022.Towards a robust CFD modelling approach for reliable hydrodynamics and mass transfer predictions in aerobic stirred fermenters Biochem. Eng. J. 181,108405. https://doi.org/10.1016/j.bej.2022.108405.

Montante G, Paglianti A., 2015. Gas hold-up distribution and mixing time in gas-liquid stirred tanks. Chem. Eng. J. 279, 648-658. https://doi.org/10.1016/j.cej.2015.05.058.

Noorman H.J., Van Winden W., Heijnen J.J., Van Der Lans R.G.J.M., 2018. Intensified Fermentation Processes and Equipment. in: RSC Green Chem. January (55), 1–41. https://doi.org/10.1039/9781788010320-00001.

Olerni, C., Jia, J., Wang, M., 2013. Measurement of air distribution and void fraction of an upwards air-water flow using electrical resistance tomography and a wire-mesh sensor. Meas. Sci. Technol. 24 (3), 035403. https://doi.org/10.1088/0957-0233/24/3/035403.

Paglianti, A., Carletti, C., Montante, G., 2017. Liquid Mixing Time in Dense Solid-Liquid Stirred Tanks. Chem. Eng. Technol. 40 (5), 862-869. https://doi.org/10.1002/ceat.201600595.

Rodgers, T.L., Gangolf, L., Vannier, C., Parriaud, M., Cooke, M., 2011. Mixing times for process vessels with aspect ratios greater than one. Chem. Eng. Sci. 66 (13), 2935-2944. https://doi.org/10.1016/j.ces.2011.03.036.

Veera, U.P., Patwardhan, A.W., Joshi, J.B., 2001.Measurement of gas hold-up profiles in stirred tank reactors by gamma ray attenuation technique. Chem. Eng. Res. Des. 79 (6), 72097, 684-688. https://doi.org/10.1205/026387601316971352.

Vrábel, P., Van Der Lans, R.G.J.M., Cui, Y.Q., Luyben, K.Ch.A.M., 1999. Compartment model approach: Mixing in large scale aerated reactors with multiple impellers. Chem. Eng. Res. Des., 77 (4), 291-302. https://doi.org/10.1205/026387699526223.

Wang, M., Dorward, A., Vlaev, D., Mann, R., 2000. Measurements of gas-liquid mixing in a stirred vessel using electrical resistance tomography (ERT). Chem. Eng. J. 77 (1-2), 93-98. https://doi.org/10.1016/S1385-8947(99)00138-2.

Zhao, D., Gao, Z., Müller-Steinhagen, H., Smith, J.M., 2001. Liquid-phase mixing times in sparged and boiling agitated reactors with high gas loading. Ind. Eng. Chem. Res., 40, 1482-1487. https://doi.org/10.1021/ie000445w.